Available online at www.sciencedirect.com
SCIENCE DIRECT®
Journal of Sound and Vibration 270 (2004) 483–494
JOURNAL OF SOUND AND VIBRATION
www.elsevier.com/locate/jsvi

On the computation of sound in free and wall-bounded domains

E.J. Avital

Department of Engineering, Queen Mary, University of London, Mile End Road, London E1 4NS, UK

Accepted 15 September 2003

Abstract

A new Dispersion-Relation-Preserving (DRP) scheme has been developed using the Lax–Wendroff methodology. Two collocated grids are placed in a staggered formation and a staggered DRP scheme is used to calculate the spatial differentiation of the propagation and convection terms. A staggered filtering scheme of a six points stencil is developed to complete the transformation from one grid to another. Existing DRP Runge–Kutta schemes are used for the time marching. Stability limits and accuracy issues are investigated using a simple 1D advection equation. The new method is then tested for monopole and quadrupole radiation, diffraction effects of an aperture in a wall, and convection effects of shear flow. All demonstrate the good accuracy and numerical stability of the new method.

1. Introduction

Computational Aeroacoustics (CAA) requires the calculation of sound over long distances with minimum amplitude and phase distortion. This rather difficult task becomes even more difficult due to the need to calculate the source at the same time. This is because of the difference in the scales between the source field and the sound field, causing the latter to have a much larger length scale and a much lower energy level, particularly in a subsonic environment. Sometimes the Green function approach can be used to tackle these issues efficiently as in basic radiation calculation [1]. However, this technique usually requires using restrictive assumptions such as parallel mean flow and/or is limited to a certain mechanism of sound generation, for example, of a low Mach number or of a high frequency. A more general method but also more computationally expensive is to march the governing equations of the sound field in time, whether they are of an acoustic analogy [2] or of an appropriate form of Euler [3] and Navier–Stokes equations [4]. This method is the subject of this paper.

E-mail address: e.avital@qmul.ac.uk (E.J. Avital).

0022-460X/$ - see front matter
doi:10.1016/j.jsv.2003.09.043

In order to achieve an efficient time-marching method, Tam and Webb [5] developed a Dispersion-Relation-Preserving (DRP) method, which includes a fourth order DRP spatial differentiation scheme for an equally spaced collocated grid. A DRP scheme for an equally spaced staggered grid was developed by Djambazov et al. [6], who also showed how to model the presence of a rigid body by using the step-wise configuration. Recently, Avital [7] developed a DRP scheme for a non-uniform staggered grid of a finite volume type in order to tackle more efficiently the difference in the length scale between the sound field and the source field.

The advantage of the staggered scheme over the collocated scheme is that it does not produce parasite short waves in the spatial differentiation and thus leads to a better numerical accuracy and stability [7]. However, the collocated DRP scheme is still required for calculating the convection terms even on the staggered grid and numerical dissipation has to be added in order to stabilize the simulation. This can be achieved by adding a dissipation term that acts mainly on the short waves, but it also requires the specification of a numerical Reynolds number. The aim of this paper is to develop a DRP method by using two collocated grids in a staggered formation and thus the staggered differentiation DRP scheme can be used for all the terms. This is actually the Lax–Wendroff methodology and here it will be extended to an optimized high order technique.

The next section develops the numerical method and examines stability and accuracy issues. Test cases are investigated in Section 3 and the work is summarized in Section 4.

2. Numerical formulation

The new method is applied to the linearized Euler equations in this work. However, initially it is easier to consider some basic issues using a simple 1D advection equation.

2.1. The 1D advection equation

Consider the following 1D advection equation:

$$\frac{\partial u}{\partial t} + c\frac{\partial u}{\partial x} = 0. \tag{1}$$

Then the basic two-steps Lax–Wendroff (LW) method is

$$u_{i+1/2}^{n+1/2} = 0.5(u_i^n + u_{i+1}^n) - 0.5\sigma(u_{i+1}^n - u_i^n), \quad \sigma \equiv c\Delta t/h, \tag{2a}$$

$$u_i^{n+1} = u_i^n - \sigma(u_{i+1/2}^{n+1/2} - u_{i-1/2}^{n+1/2}). \tag{2b}$$

h is the grid spacing and Δt is the time step. The second order in space is achieved by the staggered differentiation $(u_{i+1}^n - u_i^n)/h$ in Eq. (2a) and $(u_{i+1/2}^{n+1/2} - u_{i-1/2}^{n+1/2})/h$ in Eq. (2b), and by the staggered filtering/averaging $0.5(u_i^n + u_{i+1}^n)$ in Eq. (2a). The second order accuracy in time is achieved by using a second order Runge–Kutta (RK) marching scheme that uses time levels n and $n + 1/2$ to predict time level $n + 1$. The overall method is stable for $\sigma \leqslant 1$ and has a fourth order numerical dissipation due to the filtering in Eq. (2a).

This basic method can be extended to a high order DRP scheme by using the DRP RK schemes of Hu et al. [8] for the time marching, and staggered schemes for the spatial differentiation and

filtering, leading to

$$K^l_{i+(1-s)/2} = \Delta t F(u^n_{i+s/2} + \beta^l K^{l-1}_{i+s/2}), \quad l = 1, \ldots, p, \ s = (l-1)\%2, \tag{3a}$$

$$u^{n+1}_i = u^n_i + K^l_i, \tag{3b}$$

where % is the modulo and $F = -c\partial u/\partial x$ in the case of (1). p must be an even number and if $p = 2$ then the time marching is identical to the basic LW of (2a) and (2b). The coefficients of β^l are given in Ref. [8], which are for the two, four and six sub-time steps RK schemes. The four and six sub-time steps schemes were optimized by Hu et al. [8] in order to reduce dispersion errors and they have at least a second order accuracy.

The derivative $\partial u/\partial x$ is to be calculated by a staggered DRP scheme of a six points stencil and fourth order accuracy following Avital [7]:

$$\left.\frac{\partial u}{\partial x}\right|_{i+1/2} = \alpha_D \frac{(u_{i-1} - 27u_i + 27u_{i+1} - u_{i+2})}{24h} + (1-\alpha_D)\frac{(u_{i-2} - 125u_i + 125u_{i+1} - u_{i+3})}{120h}. \tag{4}$$

α_D is taken as 1.769304513 in order to achieve pseudo-spectral behaviour. At the odd sub-time steps ($l = 1, 3\ldots$), spatial filtering is required to calculate $u^n_{i+1/2}$. A fourth order central filter of a six points stencil can be expressed as

$$u_{i+1/2} = \alpha \frac{(-u_{i-1} + 9u_i + 9u_{i+1} - u_{i+2})}{16} + (1-\alpha)\frac{(-u_{i-2} + 25u_i + 25u_{i+1} - u_{i+3})}{48}, \tag{5}$$

where α is a constant to be used to optimize the scheme.

The goal is to achieve an optimized stable method. We have already chosen for this purpose DRP schemes for the time marching and spatial differentiation, so what is left is to optimize the filtering scheme in Eq. (5). Fig. 1(a) shows the effect of α on the filtering ratio, which is defined as the ratio between $u_{i+1/2}$ after the filtering to that before, and where u_i is taken as $\exp(\mathrm{j}kx_i)$. It is seen that the filtering ratio becomes negative in high wave numbers for $\alpha < -1.25$ and it also became larger than the one in medium wave numbers for α larger than about 1.5. Both effects are undesirable and thus α should be limited to a certain range. This range can be figured out from Fig. 1(b), which shows the effect of α and the Courant number (σ) on the stability of the method for the four sub-time steps RK method. The results shown in that figure were achieved by assuming again $u_i = \exp(\mathrm{j}kx_i)$, marching one time step and then checking if the magnitude of u^{n+1}_i was larger than one for $0 \leqslant k\Delta x \leqslant \pi$. It is seen that keeping $-6 \leqslant \alpha \leqslant 1.5$ and the appropriate limit on σ keeps the method stable. The range for α can be explained by the behaviour outlined in Fig. 1(a) and the higher than one limit for the Courant number is due to the four sub-time steps RK scheme.

Taking $u^n_i = \exp(\mathrm{j}kx_i)$ analytically leads to the relation $u^{n+1}_i/u^n_i = \exp(-\mathrm{j}kh\sigma)$. Using this relation the amplification of the amplitude and the phase error after one time step were calculated for the second order, fourth order schemes and the DRP scheme for various values of α. The results are shown in Fig. 2 for $\sigma = 0.5$.

The results show that the DRP scheme manages to suppress better the Nyquist (oddball) wave number than the other schemes. This is due to the better resolution in the spatial differentiation, leading to a better suppression in the filtering. It is an advantage since the high wave numbers are not expected to be well resolved and numerical instability usually occurs due to accumulation of energy in the high wave numbers. However, reducing α below -1.25 stops the suppression of the

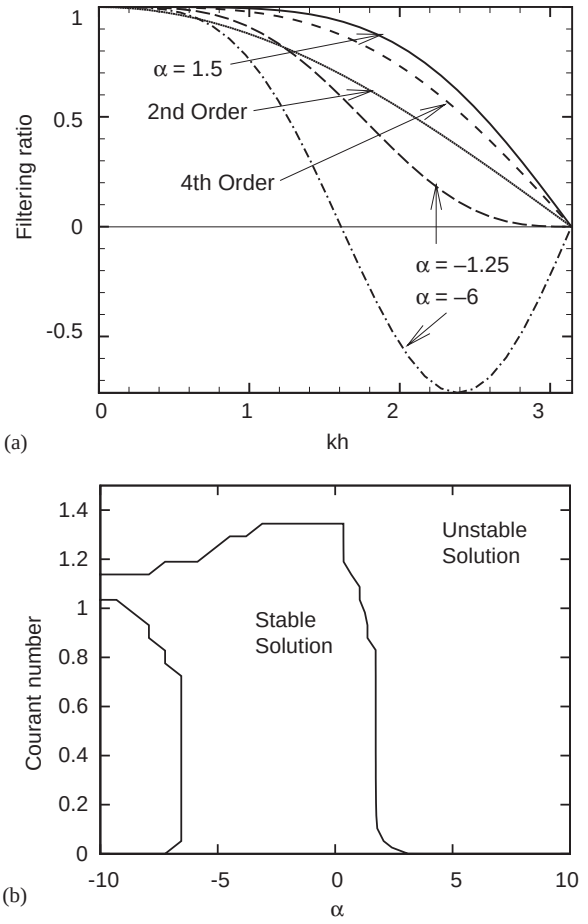

Fig. 1. The effect of α-the filtering constant on (a) the filtering ratio of (5) and on (b) the stability of the DRP method when using the four sub-time steps RK scheme of Eqs. (3a) and (3b).

high wave numbers from being monotonic, which is consistent with the finding in Fig. 1(a) of a negative filtering ratio. This is an undesired behaviour that can lead to instability as was seen in Fig. 1(b). A high positive α also keeps the phase error small as is demonstrated in Fig. 2(b), thus leading to the conclusion that α should be taken as high as possible, which is about 1.5 due to stability constraints.

To check the effect of the Courant number (σ) on the optimum value of α, the following norm was calculated for various α and σ:

$$I \equiv \left|\left| \frac{u_i^{n+1}}{u_i^n} - e^{(-jkh\sigma)} \right|\right| \equiv \frac{1}{\pi/2} \int_0^{\pi/2} \left| \frac{u_i^{n+1}}{u_i^n} - e^{(-jkh\sigma)} \right|^2 d(kh), \tag{6}$$

where $||$ in the integral denotes a complex modulus. The integration limits are due to the expectation that the resolved wave number range will be at $0 < kh < \pi/2$ [5]. The results are shown in the contour plot of Fig. 3, which shows that taking $\alpha \cong 2.5$ leads to the lowest I in the widest

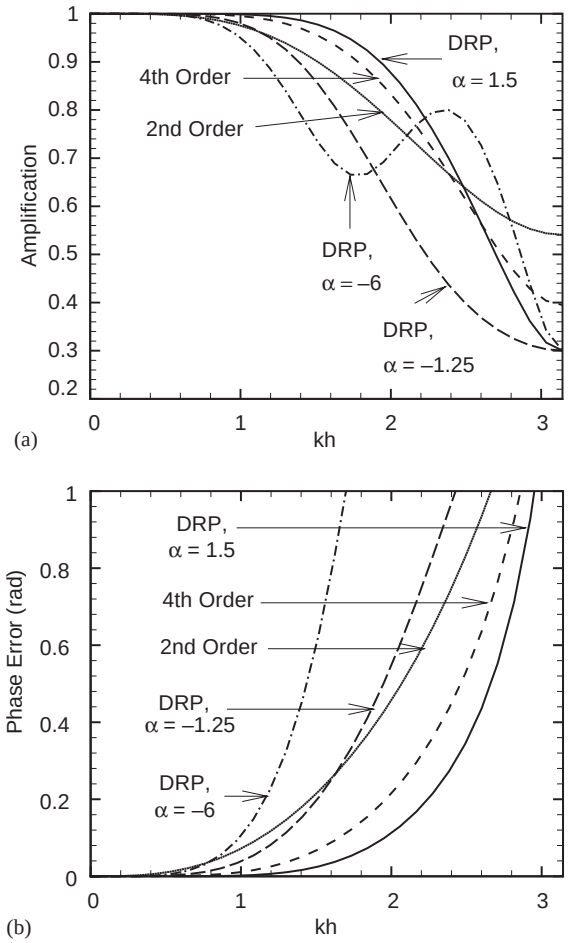

Fig. 2. The variation of (a) the amplification of the amplitude and (b) the phase error for the various numerical schemes after marching one time step of $\sigma = 0.5$ when using the four sub-time steps RK scheme.

range of σ. Unfortunately, this value of α can lead to instability according to Fig. 1(b), thus the optimum value of α should be kept as 1.5 as was concluded for the case of $\sigma = 0.5$, while minding that it should be further reduced for high σ according to Fig. 1(b).

2.2. The linearized Euler equations

The DRP method developed in Section 2.1 can also be applied to the linearized Euler equations:

$$\frac{\partial \rho}{\partial t} + \frac{\partial}{\partial x_i}(\bar{\rho} u_i + \rho \bar{u}_i) = Q, \tag{7a}$$

$$\frac{\partial(\rho \bar{u}_i + \bar{\rho} u_i)}{\partial t} + \frac{\partial}{\partial x_j}(\overline{\rho u}_i u_j + \bar{\rho} u_i \bar{u}_j + \rho \bar{u}_i \bar{u}_j) + \bar{c}^2 \frac{\partial \rho}{\partial x_i} = F_i, \tag{7b}$$

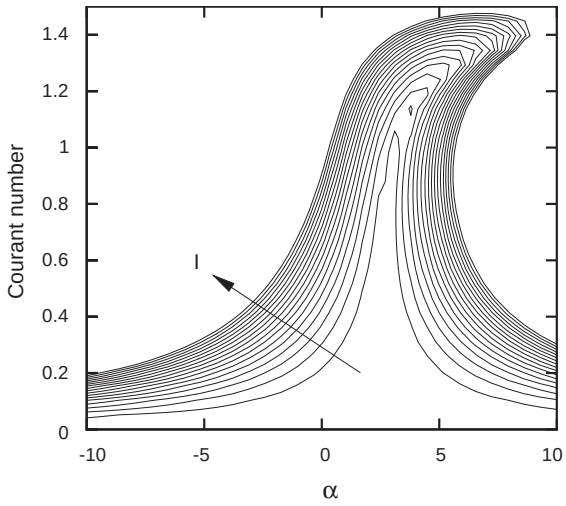

Fig. 3. The effect of α and the Courant number (σ) on the accuracy of the DRP method after one time step, where the norm I is defined in Eq. (6).

where Q is the volume source and F_i is the force source. The bar denotes a mean flow property that is calculated for example using a CFD tool and the fluctuations are assumed to be isentropic, i.e., $\partial p/\partial \rho = \bar{c}^2$. The equations can be marched in time using the schemes in Eqs. (3a) and (3b), where u_i has to be extracted from (7b) every sub-time step. The spatial differentiation and filtering are carried out as in the 1D case using (4) and (5). However, there is a need for an additional filtering in the directions normal to the direction of the differentiation in order to move between the two grids.

The effect of rigid bodies in the multi-dimensional case is of practical interest and in this work the approach of Djambazov et al. [6] is adopted, however, with some differences. As in Ref. [6] the rigid body is modelled using a step-wise configuration, assuming that the sound wave length is much larger than the length scale of any introduced roughness, which is the grid spacing. The wall conditions are of zero normal velocity and zero gradients for the tangential velocities and density. However, in order to avoid complications at corners and the use of one-sided differentiation, these conditions are implemented using a central scheme of second order accuracy. Due to this simplification, the wall conditions have to be implemented only on the grid of the odd sub-time steps and the simulation will yield the right conditions on the wall for the other grid. Furthermore, one point away from the wall the scheme can already be made fourth order normal to the wall and two points away to a full DRP accuracy. An illustration of this technique is given in Fig. 4.

The far field components behave in the leading order as plane waves governed by the 1D advection equation and hence is the importance of the analysis in Section 2.1. The performance of the new method for the entire sound field will be tested in the next section for some fundamental cases representing basic radiation, rigid body effects and convection.

3. Test cases

Numerical simulations were performed to test the performance of the new method in relatively real situations. All simulations were carried out in 1D or 2D to ease the computational burden.

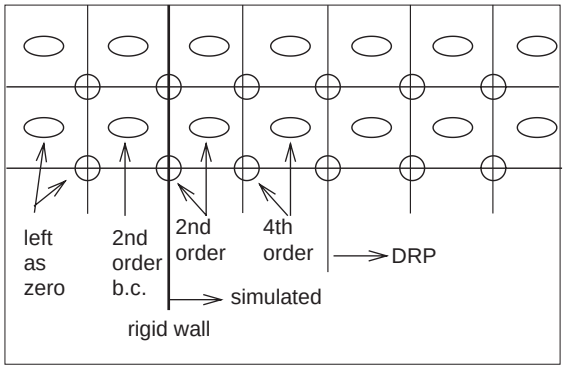

Fig. 4. Schematic description of the wall treatment. Circles denote the grid points at even sub-time steps and ellipses at odd sub-time steps. The accuracy denotes the spatial accuracy normal to the wall.

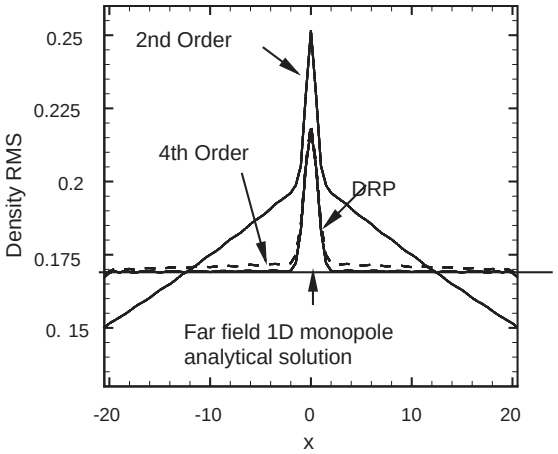

Fig. 5. The RMS of the density fluctuations generated by the 1D monopole of Eq. (8). All schemes were marched in time by the DRP four sub-time steps Runge–Kutta method.

The mean density was normalized to one and the speed of sound to 2.5. Non-reflecting boundary conditions were achieved by adding buffer zones on the sides of the computational domain [9], where a volume/body force was added to force the fluctuations to their mean value, which is zero.

The first case was to observe the sound generation by a 1D monopole with no mean flow and thus it was taken as

$$Q = \mathrm{e}^{-sx^2} \sin(\omega t), \quad F_x = F_y = 0, \tag{8}$$

where $s = 1$ and $\omega = \pi$. The Root Mean Square (r.m.s.) of the density fluctuations are shown in Fig. 5 for the second order, fourth order and the DRP schemes with a resolution of about 10 points per wavelength. As in Section 2, all schemes used the same DRP four sub-time steps RK method. The second order scheme clearly over-predicts the near field when compared with the higher order schemes and it also does not capture correctly the far field by showing a non-physical decaying field. The fourth order scheme does much better but it still shows some level of a

non-physical decay in the far field. The DRP scheme shows the best accuracy and its farfield predication is almost identical to the analytical result, which was derived by assuming a compact source. Reducing the number of grid points by half to 5 points per wavelength caused some spurious fluctuations even in the DRP scheme. Thus as in other DRP schemes that are based on a stencil of 6–7 grid points, this DRP scheme also requires about 10 points per wave length for achieving good accuracy.

Simulating a 1D dipole led to a conclusion similar to that drawn from the 1D monopole simulations. Thus, the second test case to be shown is a 2D quadrupole sound radiation. Here a lateral quadrupole was generated by specifying the sources as

$$Q = (x^2 - y^2)\mathrm{e}^{-s(x^2+y^2)} \sin(\omega t), \quad F_x = F_y = 0, \tag{9}$$

where $s = 1.5$ and $\omega = \pi$. The instantaneous density fluctuations produced by the DRP scheme are shown in Fig. 6(a), with a resolution of about 12 points per wavelength. The plot is the same as produced by the staggered grid of Avital [7]. A comparison between the various schemes is shown in Fig. 6(b) for the RMS of the density fluctuations at $y = 0$. As in the monopole case, the second order scheme over-predicts the near field and also the rate of decay of the far field, which should be of $1/\sqrt{r}$. The fourth order and the DRP schemes manage to capture correctly the energy level of the far field; however, the fourth order scheme over-predicts the near field and shows some non-physical oscillations at the edge of the source, i.e., $|x| \cong 2$. The success of both schemes to capture correctly the farfield decay, even though they were less successful in capturing the exact peaks of the near field is due to the correct prediction of the total acoustic power output of the source.

The modelling of a rigid body was tested successfully for reflection problems of a rigid plane and a sudden change in the cross-section of a duct. Here the interesting problem of diffraction by an aperture in a wall is reported. A wall was put on the right side of the 1D monopole described in Eq. (8). The distance between the wall centre to the source centre was three times the sound wavelength and the wall thickness was one-fifth of the wavelength. Fig. 7 shows the instantaneous density fluctuations for two cases, a wall with an aperture of a width of four times the wavelength and an aperture of a width of half the wavelength. The resolution is about 20 points per wavelength in order to model the wall thickness and the aperture width accurately. As expected the sound field with the wide aperture shows little diffraction, which is mostly near the edges of the aperture. Most of the sound that passes the aperture continues to propagate in relatively straight wave fronts. On the other hand, the sound field with the narrow aperture shows a much stronger diffraction effect where the wave fronts become circular after passing the aperture. A strong reflected sound wave on the left side of the wall causes a standing wave such that its front is slightly bent near the aperture due to the reflected and diffracted waves from the aperture. A more detailed and more quantitative comparison to ray acoustics in terms of reflection and diffraction effects has been performed for the problem of acoustic barriers and is reported in Refs. [10,11].

Finally, the modelling of the convection terms was tested by putting the quadrupole of (9) inside a mean parallel shear flow representing the mixing region in a subsonic jet [12]

$$\bar{u} = 0.5[1 + \tanh(b_2(Y/y - y/Y))], \quad b_2 = 0.25\,Y/\delta_2. \tag{10}$$

U is the centreline velocity, Y is the jet half-width and δ_2 is the momentum thickness. In our case Y was taken as 1, δ_2 as 0.4. The instantaneous density fluctuations are shown in Fig. 8. The plot

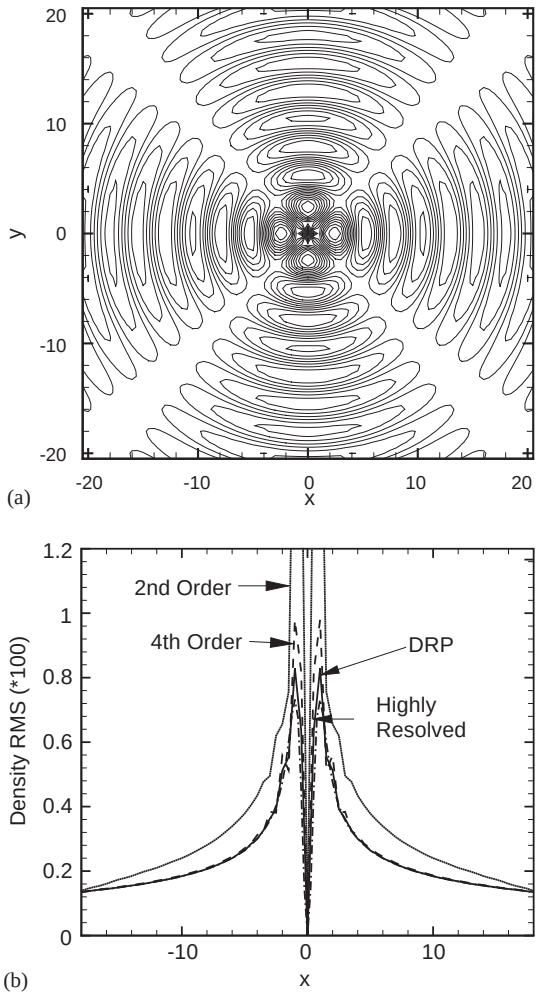

Fig. 6. Sound generation by the 2D lateral quadrupole of Eq. (9), showing (a) instantaneous density fluctuations simulated by using the DRP scheme and with 16 contour levels between ± 0.0024, and (b) the density RMS distribution along x and at $y = 0$ for the various schemes.

agrees well with the result of Avital [7], showing the generation of a cone of silence downstream due to shear refraction and the collapse of the upstream radiation due to the Doppler effect.

It should be noted that none of the reported simulations showed numerical instability as long as the stability constraints discussed in Section 2.1 were followed. This is due to the internal dissipation mechanism of the scheme that acts on the high wave numbers and which is not present in the other DRP schemes mentioned in the introduction. However, some caution has to be exercised when the convection terms are simulated in a shear flow environment. For example when the source frequency in the jet model of Fig. 8 was reduced to $St = 0.3$, strong instability waves appeared in the shear flow. This is a physical phenomenon but it also shows that the current method can produce exponentially growing fluctuations.

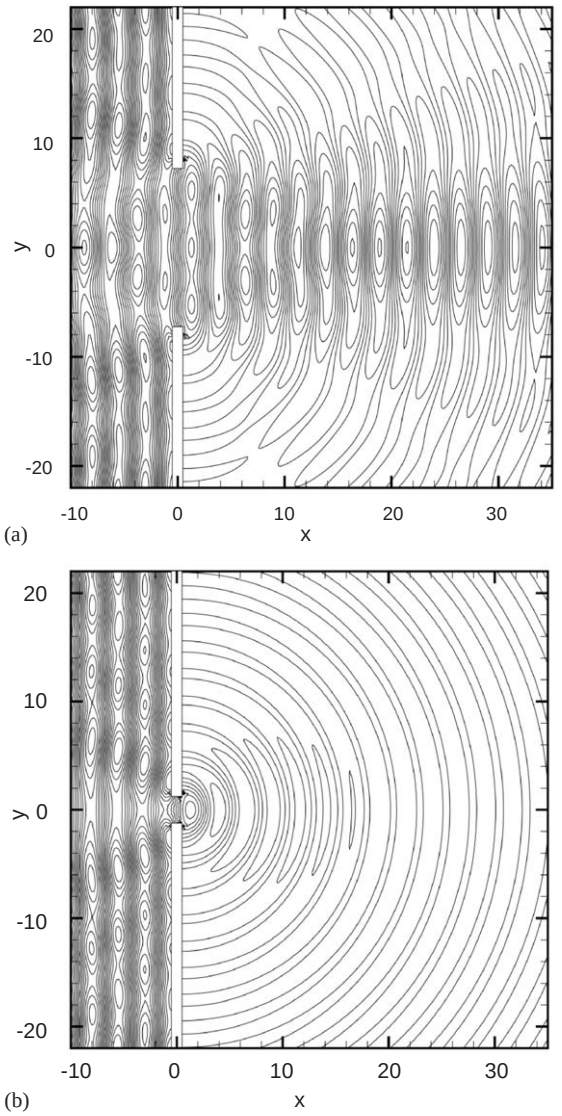

Fig. 7. Instantaneous density fluctuations generated by the monopole of Eq. (8) located at $x = -15$ and in the vicinity of a wall with an aperture with a width of (a) four times the sound wavelength and (b) half of the wavelength. There are 16 contour levels between ± 0.3.

4. Summary and outlook

A new DRP scheme for simulating sound in free and wall-bounded domains has been developed. It is based on the Lax–Wendroff methodology in which two collocated grids are placed in a staggered formation relative to each other. Existing DRP Runge–Kutta schemes are used for the time marching and an existing staggered DRP scheme of a six points stencil is used for the spatial differentiation. A new staggered filtering scheme of a six points stencil is developed and

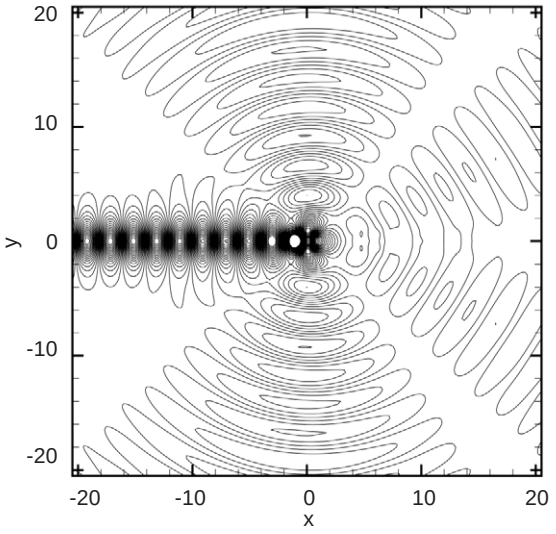

Fig. 8. Instantaneous density fluctuations generated by the quadrupole of Eq. (9) located inside the mean shear flow of Eq. (10) and with 32 contour levels between ± 0.012.

optimized while taking into account stability constraints. The new scheme has been investigated for the 1D advection equation and the linearized Euler equations. Basic radiation from monopoles and quadrupoles as well as diffraction and convection effects have been simulated to investigate the capability of the new method.

Further computational efficiency can be gained if non-uniform grids are used to cluster points in the vicinity of sources and rigid bodies with small length scales as the wall in Fig. 7. This can be achieved by mapping a uniform computational domain to a non-uniform physical domain. For example the algebraic mapping of Avital [7] maps a uniform grid to two blocks of uniform grids with a smooth transition between them. It has been planned to use this mapping and a variation of the current DRP method to model the Navier–Stokes equations in order to investigate flows dominated by feedback mechanism. Further use of the new method has been in studying acoustic barriers as mentioned before and these results are reported in Refs. [10,11].

Acknowledgements

The author thanks the Engineering and Physical Sciences Research Council (EPSRC) for their support of the aeroacoustics research programme under Grant GR/N36097/01 and for providing access to computing facilities under Grant GR/R64957/01.

References

[1] E.J. Avital, N.D. Sandham, K.H. Luo, R.E. Musafir, Calculation of basic sound radiation of axisymmetric jets by direct numerical simulation, *American Institute of Aeronautics and Astronautics Journal* 97 (2) (1999) 161–168.

[2] X. Jiang, E.J. Avital, K.H. Luo, Direct computation and aeroacoustic modelling of a subsonic axisymmetric jet, *Journal of Sound and Vibration* 270 (3) (2004).
[3] C. Bailly, D. Juve, Numerical solution of acoustic propagation problems using linearized Euler equations, *American Institute of Aeronautics and Astronautics Journal* 38 (1) (2000) 22–29.
[4] E.J. Avital, N.D. Sandham, K.H. Luo, Mach wave radiation by mixing layers Part I: analysis of the sound field, *Theoretical and Computational Fluid Dynamics* 12 (2) (1998) 73–90.
[5] C.K.W. Tam, J.C. Webb, Dispersion-relation-preserving finite difference schemes for computational acoustics, *Journal of Computational Physics* 107 (1993) 262–281.
[6] G.S. Djambazov, C.H. Lai, K.A. Pericleous, Staggered-mesh computation for aerodynamic sound, *American Institute of Aeronautics and Astronautics Journal* 38 (1) (2000) 16–21.
[7] E.J. Avital, Optimized differentiation schemes on non-uniform grids for computational aeroacoustics, *Journal of Computational Acoustics* 10 (3) (2002) 1–15.
[8] F.Q. Hu, M.Y. Hussaini, J.L. Manthey, Low-dissipation and low-dispersion Runge–Kutta schemes for computational acoustics, *Journal of Computational Physics* 124 (1996) 177–191.
[9] E.J. Avital, Direct and large eddy simulation of compressible open cavity flows, in: B.J. Geurts, R. Friedrich, O. Metais (Eds.), *Direct and Large Eddy Simulation IV*, Kluwer Academic Publishers, Dordrecht, 2001, pp. 213–220.
[10] D.F.P. Pazos, R.E. Musafir, E.J. Avital, Assessment of the Kurze–Anderson approach in the prediction of barrier insertion loss near a reflecting ground, *XX Meeting of the Brazilian Acoustical Society*, Rio de Janeiro, October 2002.
[11] D.F.P. Pazos, R.E. Musafir, E.J. Avital, Assessment of adequacy of ray acoustics approach for prediction of barrier insertion loss in the presence of a reflecting ground, *First Pan-American/Iberian Meeting on Acoustics*, *Acoustical Society of America*, Cancun, December 2002.
[12] A. Michalke, Survey on jet instability, *Progress in Aerospace Sciences* 24 (1984) 159–169.